







Examination of photon strength functions and nuclear level density in ^{196}Pt from the γ -ray spectra measured at the DANCE facility

N. Simbirtseva ^{1,2} M. Krtička ^{3,*} R. F. Casten ^{4,5} A. Couture,⁶ W. I. Furman ¹ I. Knapová ³
J. M. O'Donnell,⁶ G. Rusev,⁶ J. L. Ullmann,⁶ and S. Valenta ³

¹Joint Institute for Nuclear Research, Joliot Curie 6, Dubna 141980, Russia

²Institute of Nuclear Physics, Almaty 050032, Republic of Kazakhstan

³Faculty of Mathematics and Physics, Charles University, 180 00 Prague, Czech Republic

⁴Wright Lab, Yale University, New Haven, Connecticut 06520, USA

⁵Michigan State University-Facility for Rare Isotope Beams (MSU-FRIB), East Lansing, Michigan 48823, USA

⁶Los Alamos National Laboratory, Los Alamos, New Mexico 87545, USA



(Received 15 November 2019; accepted 21 January 2020; published 7 February 2020)

Background: The nuclear level density (NLD) and photon strength functions (PSFs) are necessary quantities for calculating the interaction of photons with nuclei, in particular the reaction cross sections. As such, they are important especially in nuclear astrophysics and in the development of advanced nuclear technologies.

Purpose: The presence of a resonancelike structure in the $E1$ PSF at γ -ray energy of about 5.5 MeV was reported in γ -soft $A \approx 200$ nuclei from several experimental techniques. However, as data from different experiments are not fully consistent, additional information on PSFs in this region is of great interest. In addition, present PSF models have difficulties to describe resonancelike structures for energies below the neutron separation energy S_n . There are also open questions about the energy and parity dependence of the NLD.

Methods: The γ rays following the radiative neutron capture on ^{195}Pt s -wave resonances were measured with the highly segmented γ -ray calorimeter Detector for Advanced Neutron Capture Experiments at the Los Alamos Neutron Science Center. The γ -ray energy spectra for different multiplicities were gathered for several resonances of both possible spins.

Results: The γ -ray energy spectra were analyzed within the statistical model and allowed us to get information about the NLD and PSFs in ^{196}Pt . Neither the PSFs from any previous experiment nor any available PSFs models are able to describe our spectra. We were able to find PSFs and NLD that reasonably describe experimental spectra and impose various restrictions on these quantities.

Conclusions: The presence of a resonancelike structure in the $E1$ PSF at a γ -ray energy of about 5.6 MeV is confirmed. The constant temperature energy dependence is favored for a NLD with a significant parity dependence up to an excitation energy of at least 4 MeV. The preferred $M1$ PSF shape is close to a Lorentzian tail of the spin-flip resonance.

DOI: [10.1103/PhysRevC.101.024302](https://doi.org/10.1103/PhysRevC.101.024302)

I. INTRODUCTION

With presently available experimental techniques the complete spectroscopic data in medium- and heavy-mass nuclei can be obtained only for levels at lowest excitation energies below at most up to about 2 MeV in even-even nuclei away from closed shells. These limitations originate mainly from the nuclear level density (NLD) rapidly increasing with excitation energy. Properties of medium-weight and heavy atomic nuclei at higher excitation energies are then usually described using the statistical model in terms of the NLD and a set of photon strength functions (PSFs) for different transition types. These quantities are necessary for calculations of cross sections in all reactions involving photons and are important

especially in nuclear astrophysics [1,2] and in the development of advanced nuclear reactors [3].

The study of these quantities is important especially in regions where they show significant irregularities or, in the case of PSFs, presence of resonance structures below neutron separation energies. One of these regions appears for γ -soft $A \approx 200$ nuclei, where previously measured data indicate a presence of a resonance at $E_\gamma \approx 5.5$ MeV in a PSF [4–9]. As experimental data from average resonance capture indicate dominance of $E1$ strength at these energies in this mass region (see latest compilation [10] and references therein) and the resonance is significantly weaker than the dominant giant electric dipole resonance (GEDR), the observed structure is usually referred to as pygmy $E1$ resonance. The pygmy resonance was observed in many isotopes across the nuclei chart [11].

Low-lying dipole resonances, i.e., pygmy $E1$ and scissors $M1$ resonances, are usually not reflected in widely used PSFs

*Corresponding author: krticka@ipnp.troja.mff.cuni.cz

models, such as those compiled in RIPL-3 [12], or recently proposed systematic based on the HFB+QRPA calculations [13]. However, their presence may have serious implications for heavy-element nucleosynthesis [14].

Important information on PSFs and NLD can be obtained from an analysis of coincident γ -ray spectra measured in the decay of isolated neutron resonances. In this paper we report on results from the analysis of the so-called multistep cascade (MSC) spectra gathered for s -wave resonances in radiative neutron capture on ^{195}Pt . The γ -ray spectra were measured with the Detector for Advanced Neutron Capture Experiments (DANCE) [15,16]. This highly segmented, highly-efficient γ -ray calorimeter, consisting of 160 BaF_2 crystals, is installed at the pulsed neutron beam at Los Alamos Neutron Science Center (LANSCE) at Los Alamos National Laboratory.

In Sec. II we describe the experimental technique to measure the MSC spectra with the DANCE calorimeter as well as modeling of the statistical γ cascades. Information about the PSFs and NLD that can be extracted from the measured MSC spectra is presented in Sec. III. Consistency of observed size of fluctuations in spectra from different resonances with predictions of the statistical model is then discussed in Sec. IV and a summary is given in Sec. V.

II. EXPERIMENT AND DATA PROCESSING

A. Experimental setup

A 30-h-long neutron-capture experiment with an enriched Pt sample was performed at neutron flight path 14 at LANSCE [17,18]. A white spectrum of spallation neutrons was produced by irradiation of a tungsten target with 800-MeV protons with a repetition rate of 20 Hz. The low-energy part of the neutron-flux distribution is enhanced by a water moderator. A comprehensive description of the experimental setup can be found in Refs. [15,16,19,20]. Here we restrict ourselves only to basic features and details specific to the Pt measurement.

A self-supporting $1/4 \times 1/4$ in. square metal foil sample of Pt enriched to 97.29% in ^{195}Pt with total mass of 35 mg was located at the center of the DANCE detector at a distance of 20.25 m from the spallation neutron source.

The DANCE consists of 160 BaF_2 crystals which cover a solid angle of $\approx 3.5\pi$ with an efficiency of 86% for a single photon with $E_\gamma = 1$ MeV [21]. The energy resolution is about 16% and 7% for 1 and 6 MeV γ rays, respectively. A ^6LiH shell about 6 cm thick is placed between the sample and the crystals to absorb a significant fraction of neutrons that scatter from the sample and would otherwise strike the crystals. The energy of neutrons impinging on the sample was determined using the time-of-flight (TOF) technique. Events corresponding to neutron energies $E_n > 9$ eV were recorded.

The DANCE acquisition system [20] is based on digitization of signals from all 160 BaF_2 detectors using Acqiris DC265 digitizers with a sampling rate of 500 mega samples per second. Intensities of the fast (decay time ≈ 600 ps) and slow (decay time ≈ 600 ns) components of the scintillation signal from each BaF_2 detector are collected independently. The ratio of these two signal components is then used for

discrimination against the α background from natural radioactivity of Ra in the BaF_2 crystals [16]. A precise time stamp of γ -ray arrival is also stored and in this analysis the signals from individual detectors that arrive within 10 ns are considered to belong to the same event.

The energy calibration of the individual DANCE crystals was performed with a combination of γ -ray sources ^{137}Cs , ^{88}Y , ^{22}Na and the intrinsic radioactivity in the BaF_2 crystals due to a small amount of ^{226}Ra contaminant and its daughters. The latter calibration was conducted on a run-by-run basis to provide the energy alignment of all crystals in the off-line analysis.

B. Data reduction

The experimental approach is similar to that presented in Ref. [22] and only its most important features are listed below.

An emitted γ ray does not necessarily deposit its full energy in a single crystal, but rather several, often neighboring, BaF_2 crystals [19]. We combined all contiguous crystals that fired during an event into *clusters* and considered each cluster as the response of the detector array to a single γ ray. The number of clusters observed in an event is called the *cluster multiplicity* M . Although we use the cluster multiplicity, the conclusions presented here do not depend one whether the crystal or the cluster multiplicity is used.

Only events corresponding to strong, well-resolved resonances—identified from the TOF spectrum—with sufficient statistics and unambiguously known spin were analyzed. The relevant part of the TOF spectrum is shown in Fig. 1 after transformation to the neutron-energy scale. Sufficiently strong and well-resolved s -wave resonances (with $J^\pi = 0^-$ or 1^-) are observed only for $E_n \lesssim 600$ eV. In total we were able to get spectra from 5 and 11 $J^\pi = 0^-$ and 1^- resonances, respectively. The neutron energy regions used in the analysis are indicated in Fig. 1.

Spectra of sums of deposited γ -ray energies, hereafter called *sum-energy spectra*, are shown for $M = 2-4$ in Fig. 2 for a few resonances. The spectra, after background subtraction described below, are normalized to the same total number of events of $M = 3-7$ in the sum-energy range $E_\Sigma = 7-8$ MeV corresponding to the neutron separation energy $S_n = 7.92$ MeV.

Each sum-energy spectrum consists of a peak near S_n , which corresponds to detection of nearly all γ -ray energy emitted in a cascade following neutron capture, and a continuum formed by events where a part of the emitted γ -ray energy escapes the detection. The intensity at $E_\Sigma \lesssim 3$ MeV in $M \leq 3$ spectra may have a strong background contribution coming from various sources [16]. There is also a background contribution at higher E_Σ from capture of scattered neutrons in Ba of the detector crystals. As two Ba isotopes have S_n above 8.5 MeV, this contribution is usually visible in lower multiplicities for energies above the peak near S_n of the isotope of interest [22,23], located at ≈ 7.7 MeV in the case of ^{196}Pt . As evident from Fig. 2 this background is virtually absent in the Pt resonances adopted in the analysis. Nevertheless, using the spectra from neighboring off-resonance regions this very small background above $E_\Sigma \approx 3$ MeV was subtracted.

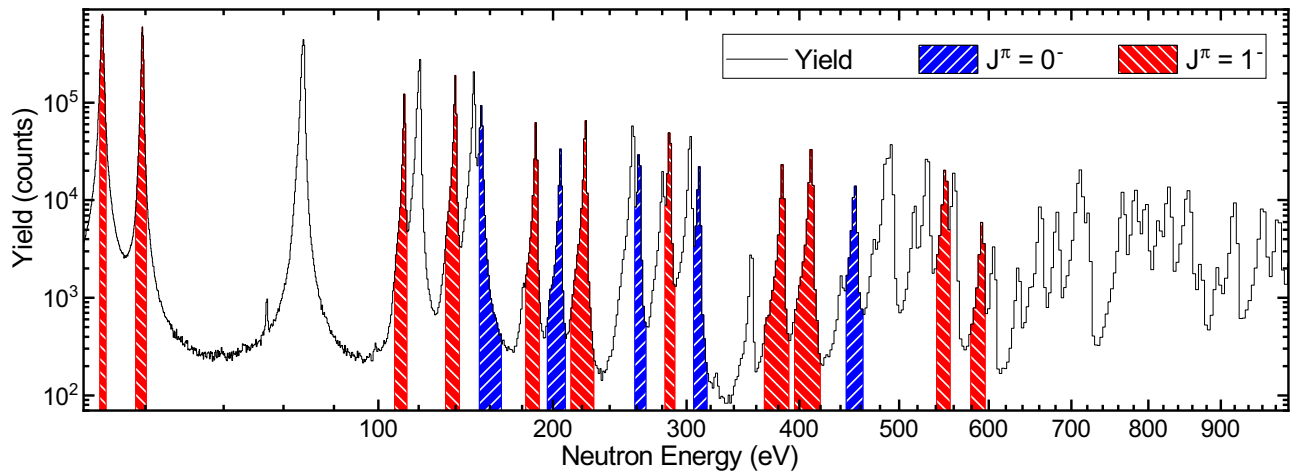


FIG. 1. Number of detected γ cascades as a function of neutron energy for events with $M > 1$ and $E_{\Sigma} = 7-8$ MeV. The resonances from capture on other Pt isotopes ($^{192,198}\text{Pt}$ at 53 and 96 eV, respectively) are barely visible due to the selection criteria on M and E_{Σ} . The hatched intervals indicate neutron energies used in the analysis.

Bumplike structures at $E_{\Sigma} \approx 2$ and 6 MeV in the sum-energy spectra of some resonances surely come from incomplete detection of γ cascades from ^{196}Pt as very similar structures are observed also in the simulations described below.

Events with deposited sum energy $E_{\Sigma} = 7-8$ MeV were used to construct the *experimental MSC spectra*. For a given

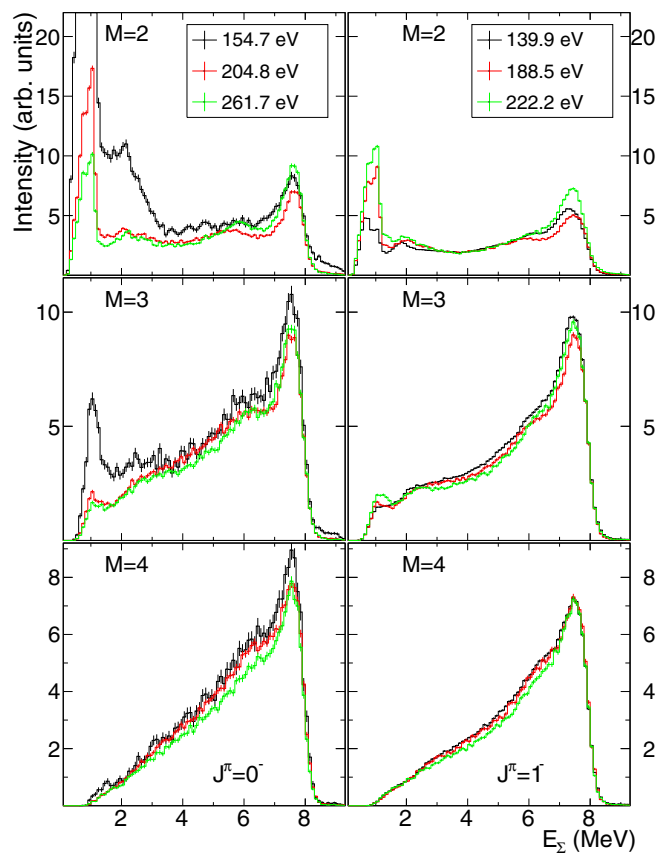


FIG. 2. Sum-energy spectra for $M = 2-4$ events of three 0^- and three 1^- resonances. The background was not subtracted to show its contribution in different resonances.

resonance, an experimental MSC spectrum for multiplicity M was constructed by incrementing counts in M bins corresponding to the γ energies deposited in the M individual clusters within an event. In other words, to better visualize the multiplicity and energy makeup of the registered events, we sort the events by multiplicity and then plot a spectrum of all individual γ energies within the events. A bin width of 100 keV, which is close to the energy resolution of crystals for low E_{γ} , was chosen. The experimental MSC spectra inherit the normalization of sum-energy spectra. It turns out that the results do not depend on the exact sum-energy range used for construction of MSC spectra provided that the events from the peak near S_n are considered. A background contribution from the scattered-neutron capture on Ba was subtracted using off-resonance regions as in the case of the sum-energy spectra. The background subtraction significantly changes only the $M = 1$ experimental MSC spectra. Examples of a few background-subtracted experimental MSC spectra for resonances with both possible spins are plotted in Fig. 3.

We were able to verify most resonance spin assignments from [24] with the help of the multiplicity-based method [25] combined with the characteristic shapes of experimental MSC spectra. The resonances entering the analysis are those for which the combined information on spin assignment unambiguously confirmed the one from [24]. As can be seen in Fig. 2 the sum-energy spectra practically coincide for $M \geq 3$ no matter the resonance spin, which is likely a consequence of the spin difference between the resonances and ground state being only 0 or 1. On the other hand, the intensities at the S_n peak in $M = 2$ spectra exhibit sizable fluctuations, which is a manifestation of strong fluctuations of a few high- E_{γ} primary transitions; see $M = 2$ MSC spectra in Fig. 3. It turns out that the shapes of MSC spectra for $M = 2-4$ differ for resonances of different spins; see Figs. 3 and 4. The difference stems mainly from the absence of $J^{\pi} = 1^+$ states at excitation energies below about 2 MeV. These are the only states expected to be strongly fed from $J^{\pi} = 0^-$ resonances via primary transitions.

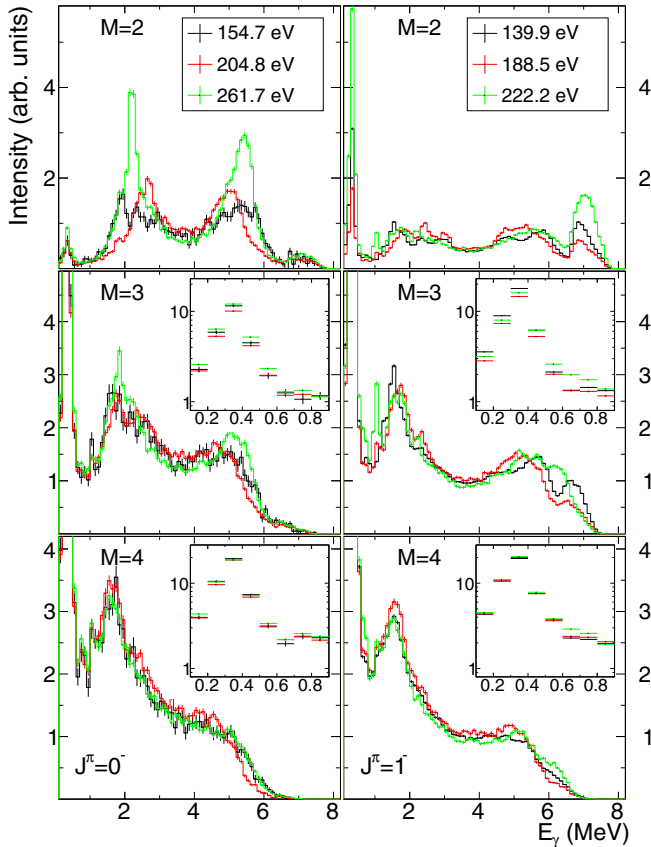


FIG. 3. Experimental MSC spectra for $M = 2-4$ of three 0^- and three 1^- resonances. The same resonances as in Fig. 2 are shown.

As mentioned above, the $M = 2$ MSC spectra dominantly consist of cascades via relatively high- E_γ primary transitions to an intermediate level that subsequently decays to one of the three lowest-lying levels.¹ The number of available intermediate levels below an excitation energy of about 3 MeV is so low, especially for primary transitions from 0^- resonances, that we can observe individual primary transitions. Spectra from individual resonances in Fig. 3 show that strong primary transitions feed different intermediate levels and that the fluctuations of primary transition intensities to the same intermediate levels from different neutron resonances are sizable. This feature points towards an enhancement of (primary) transitions with $E_\gamma \approx 5-6$ MeV in terms of PSFs, not towards nonstatistical, common structural effect in different resonances. The presence of resonances with similar structure would manifest itself via strong primaries to the same intermediate levels. Furthermore, these observed differences in the MSC spectra of individual resonances are expected in the statistical model as a consequence of Porter-Thomas (PT) fluctuations [26] of primary intensities.

¹The available sum energies for the cascades to the ground state and first two excited states are 7.92, 7.57, and 7.23 MeV, respectively, which all fall into the chosen interval $E_\Sigma = 7-8$ MeV. The cascade is registered as an event terminating at the excited state when its decay to the ground state escapes detection.

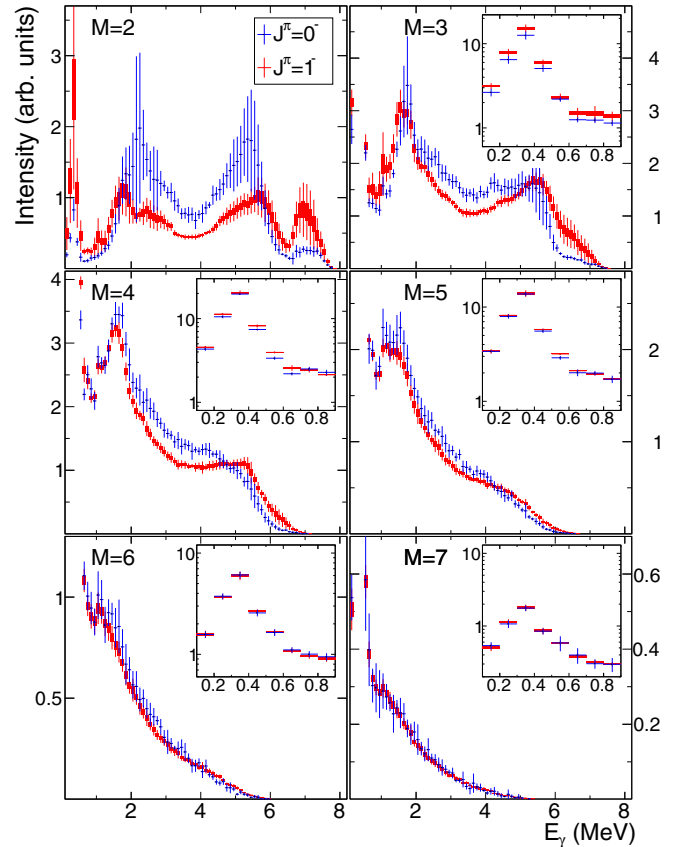


FIG. 4. Mean experimental MSC spectra. For $J^\pi = 1^-$ the full rectangle gives I_{exp} with its uncertainty while the larger error bar represents the expectation value of ϕ_{exp} . The average \pm one standard deviation is plotted for $J^\pi = 0^-$. For details see Sec. II B and Sec. 1 of the Appendix.

For comparison of experimental data with model predictions, we decided not to use spectra from individual resonances but we constructed the *mean experimental MSC spectra*. The mean experimental MSC spectra better capture the average characteristic features of the decay. The details are given in Sec. 1 of the Appendix.

The mean experimental MSC spectra for both resonance spins and $M = 2-7$ are shown in Fig. 4. For $J^\pi = 1^-$ we used $L_{\text{exp}} = 11$ individual resonances; the uncertainty of I_{exp} is displayed as a full rectangle while ϕ_{exp} is represented by the larger error bar ($I_{\text{exp}} \pm \phi_{\text{exp}}$ is drawn). Since we were not able to gather the spectra for more than five resonances with $J^\pi = 0^-$, we calculated the mean experimental MSC spectra as a simple average and standard deviation for this resonance spin; the average \pm one standard deviation is plotted. There are virtually no events with $M > 8$.

C. Simulated MSC spectra

The MSC spectra are products of a complex interplay between the PSFs, NLD, and a nontrivial detector response. As a result, there is no easy way to extract the PSFs and the NLD directly from the experimental MSC spectra. To learn about these quantities we thus adopted a trial-and-error

approach—the simulated MSC spectra obtained assuming various PSFs and NLD models were compared with their experimental counterparts. The comparison allowed us to reject many model combinations and select those giving a reasonable description of the experimental spectra.

Simulations of individual γ cascades deexciting neutron resonances with specific J^π were performed utilizing the Monte Carlo DICEBOX algorithm [27,28]. The response of the detector to individual cascades was then obtained from the Monte Carlo GEANT4-based code [19]. The use of the DICEBOX algorithm allows correct treatment of the PT fluctuations [26] of individual transition intensities as well as artificial fluctuations due to the random discretization of the NLD. Simulations were performed for many different combinations of models of NLD and $E1$, $M1$, and $E2$ PSFs, below labeled as f_{E1} , f_{M1} , and f_{E2} , respectively. As the description of the γ decay via the statistical approach is surely not adequate at the lowest excitation energies; the information on the level scheme was taken from [29] below the critical energy $E_c = 1.88$ MeV unless specified otherwise. There are only a few uncertainties in the level scheme below 1.88 MeV, which have negligible influence on the results of our simulations. An increase of E_c introduces significantly more uncertainties in the low-lying level scheme without any improvement in the description of the related regions of MSC spectra; E_c lower than 1.88 MeV enhances the fluctuations at the edges of simulated MSC spectra without having any positive effect.

More details on the DICEBOX algorithm, including the calculation of the measures of experimental observables, are given in Sec. 2 of the Appendix.

We would like to note that for normalization of simulated spectra, as in the case of experimental ones, we need only one common normalization factor for all M . We thus have not only information on spectral shapes of individual M but also on the multiplicity distribution of detected cascades. The comparison of the spectra is not shown in the figures below for $M \geq 6$ as spectral shapes do not show interesting structures, see Fig. 4, and do not provide any additional restrictions apart from reflecting the multiplicity distribution. The multiplicity distribution is in some cases used when discussing the acceptability of models in Sec. III. As in the case of experiment, there are virtually no events with $M > 8$.

To correctly statistically quantify the degree of agreement between the simulated and experimental MSC spectra, enormously time-consuming simulations with an extremely large number of suprealizations would be needed as contents of individual bins in MSC spectra are mutually correlated in a very complicated fashion and the corresponding correlation matrix is *a priori* not known. As a consequence, within the search for suitable PSFs and NLD models the degree of agreement was checked only visually.

It is to be stressed that the predicted spectra are not sensitive to the absolute values of PSFs if the E_γ -dependent ratios of PSFs for different transition types are kept the same. So, we are rather probing the energy dependence of PSFs and relative contribution of various transition types than the PSFs absolute values. The only quantity from simulations that depends on the absolute PSFs values is the total radiative width.

III. TEST OF NUCLEAR LEVEL DENSITY AND PHOTON STRENGTH FUNCTIONS MODELS

Mean experimental MSC spectra were compared to predictions based on many different combinations of PSFs and NLD models. As a first step in Sec. III B we checked the acceptance of several global models available in the literature. Further in Sec. III C we tested the PSFs based on available experimental data. Finally, we tried to fine-tune the PSFs and checked the influence of certain features in the PSFs and NLD on predicted spectra; see Sec. III D. In total several hundreds of different PSFs and NLD combinations were tested. The key results of these simulations are presented in this section. Although we compare MSC spectra mostly for 1^- resonances, a very similar degree of agreement for all presented models is obtained also for spectra from 0^- resonances.

A. Nuclear level density models and data

Tested NLD models and experimental data² from measurement at the Oslo Cyclotron Laboratory [30] are compared in Fig. 5. The constant-temperature (CT) and back-shifted Fermi-gas (BSFG) models are taken from [32]. The model labeled “Oslo” consists of, in accord with the original work [30], interpolation through the Oslo experimental points followed by extrapolation above 6 MeV by the CT formula and the spin distribution adopted from [32]. The NLD calculation labeled “Combinatorial” is available as the tabulated energy-dependent NLD for levels with each spin and parity coming from the Hartree-Fock-Bogoliubov (HFB) plus combinatorial method [33].

With a few exceptions of high-spin levels (which play a marginal role in the decay of s -wave resonances) there are no known levels with negative parity below an excitation energy of about 2 MeV [29]; a significant dominance of positive parity levels is thus expected also in the region above E_c . For simulations with the CT, BSFG, and Oslo models we have introduced the parity dependence of NLD in the form proposed in Ref. [34] which gives the fraction of levels with positive parity $F(\pi = +)$ with respect to total NLD at excitation energy E as

$$F(\pi = +) = \frac{1}{2} \left(1 + \frac{1}{1 + \exp [C_\pi (E - \Delta_\pi)]} \right). \quad (1)$$

We usually adopted $\Delta_\pi = 3$ MeV and $C_\pi = 1$ MeV⁻¹. There is virtually no parity dependence for an excitation energy above about 5.5 MeV for this parameter choice. We tested also several other choices of Δ_π and C_π as well as NLD which are parity-independent above E_c . The influence of the NLD parity dependence is discussed in Sec. III D 2. The contribution of levels with both parities is for low excitation energies indicated for the CT model [with parity dependence given by Eq. (1)] and the combinatorial NLD in Fig. 5(b).

Even-even nuclei show staggering between odd and even spins at low excitation energies [35]. We adopted the staggering of the form proposed in Refs. [32,35], which linearly

²For details about the procedure of normalization (and extrapolation) of NLD experimental data in the Oslo method see Refs. [30,31].

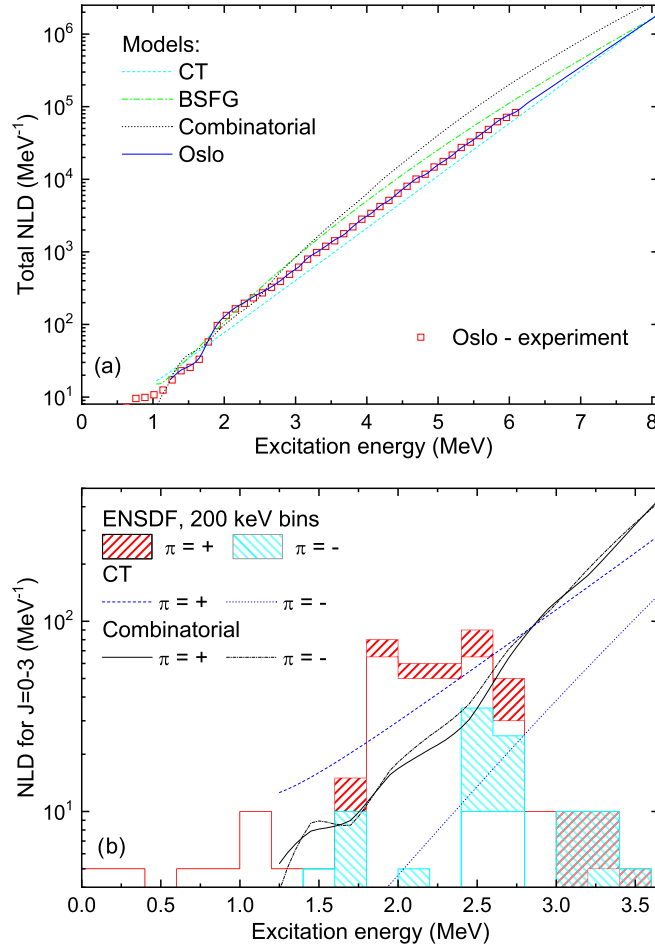


FIG. 5. Nuclear level densities used in simulations in comparison with experimental data. Total NLD is shown and compared with the Oslo data [30] in (a). The NLD of $J = 0-3$ and both parities for the CT model and Combinatorial calculation is compared to ENSDF data [29] in (b). Hatched areas reflect the minimum and maximum allowed number of levels with given parity in a 200-keV bin from [29]. The constant-temperature (CT) and back-shifted Fermi-gas (BSFG) models are from [32], combinatorial NLD from [33].

decreases with excitation energy with maximum effect below 1 MeV and vanishing at 4 MeV. Unless specified otherwise, the simulations presented below were made with the Oslo model of NLD with the above-given parity dependence and staggering as proposed in Ref. [32].

B. Global photon strength functions models

We started with a comparison of the mean experimental MSC spectra to predictions based on the PSFs models that are traditionally used.³ Predictions from two such models, presented by lines in Fig. 6(a), are shown in Fig. 7

³In all model combinations (not only those discussed in this subsection) we adopted for $E2$ PSF the single-particle (constant) model with $f_{E2} = 1 \times 10^{-10} \text{ MeV}^{-5}$. The contribution of $E2$ transitions is always small and has a negligible impact on the results.

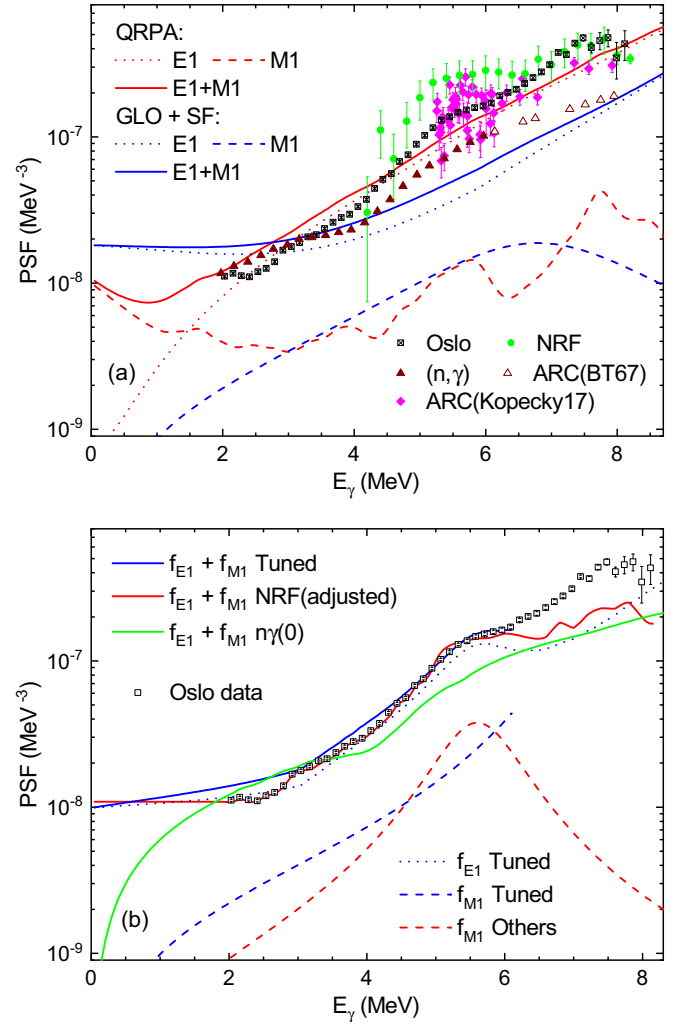


FIG. 6. Experimental data on PSFs from a few methods, that are available for ^{196}Pt , and models exploited in this work. The PSFs of two widely used models, described in Sec. III B, corresponding to primary transitions are shown in (a). The additional tested PSFs combinations, introduced in Secs. III C and III D, are shown in (b). The sources of experimental data are Oslo [8], NRF [7], (n, γ) [37], ARC (BT) [38], ARC (Kopecky) [10].

1^- resonances. One of them consists of the widely used generalized Lorentzian (GLO) model for $E1$ and the spin-flip (SF) standard Lorentzian resonance model for $M1$ PSF [12]. The other model labeled as “QRPA” is based on the QRPA + HFB calculations with the D1M force [36] for both $E1$ and $M1$ PSFs to which a “low-energy enhancement” is added as proposed by the systematics in Ref. [13]. The presented simulation using the QRPA model was made with the combinatorial NLD.

The MSC spectra predicted with these two models do not coincide with the experiment; see Fig. 7. In reality, several different NLD models were tested in combination with these two PSFs models. Use of any NLD model does not help to reduce the disagreement between simulated and experimental MSC spectra indicated in Fig. 7. Specifically, none of the model combinations is able to predict significant bumps in the

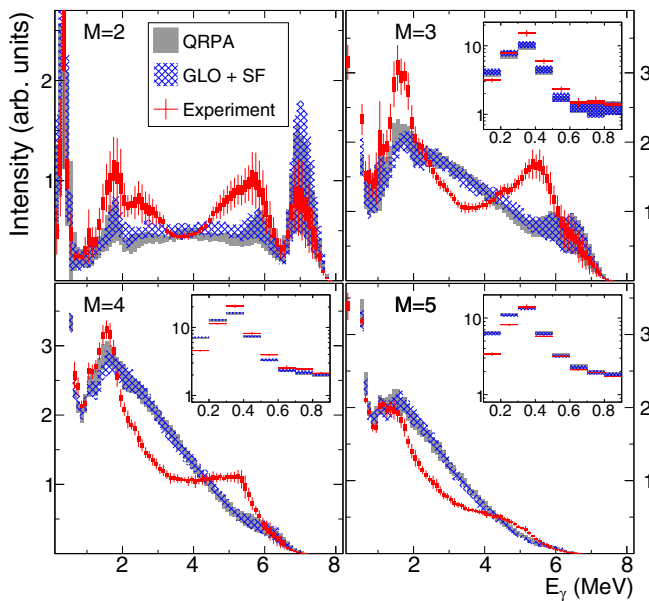


FIG. 7. Comparison of the mean experimental MSC spectra from 1^- resonances with the predictions for the two models described in Sec. III B. The symbols for experimental data are the same as in Fig. 4. The simulated bands correspond to $\mu \pm \sigma$ as introduced in Sec. II C and Sec. 2 of the Appendix.

MSC spectra near 5.6 MeV due to the lack of extra strength, such as a pygmy resonance, in the $E1$ PSF.

C. Photon strength functions based on available experimental data

Information on PSFs in ^{196}Pt or nuclei with very similar mass from several different experimental techniques can be found in the literature. Data for ^{196}Pt are shown in Fig. 6. They come from nuclear resonance fluorescence measurements from γELBE [7], preliminary analysis of $^{195}\text{Pt}(d, p\gamma)$ reaction with the Oslo method [8], and from the (n, γ) reaction. As for the (n, γ) data, there are two data sets from the 1960s which were compiled in Ref. [4]. One of them comes from the spectrum fitting method of the singles γ -ray spectrum [37] and the other one from the average resonance capture (ARC) measurement [38]. There is also a data set from newer ARC measurement [10,39]; all transitions in this data set are assumed to be of $E1$ character.

As mentioned above, simulations with PSFs of identical shape, that differ only in the absolute value, yield exactly the same MSC spectra. Considering that the absolute normalization of PSFs deduced from many experiments, including the spectrum fitting from (n, γ) and Oslo methods, is nontrivial, below we consider arbitrary normalizations with fixed shapes for discussion purposes. Multiplying the NRF experimental values from Ref. [7] by 0.6 brings this data set on top of Oslo (and newer ARC) data at $E_\gamma \approx 5.5$ MeV. The multiplication of (n, γ) data from [4] by 1.5 would match the other data sets at $E_\gamma \approx 4$ –5 and ≈ 6 MeV, pull the (n, γ) data significantly above the Oslo data for $E_\gamma = 2$ –4 MeV, and put the ARC data

from [38] in a good agreement with newer ARC data from [10,39].

All these data (perhaps with the exception of the ARC data from [10,39]) really indicate a presence of a resonancelike structure near 5.6 MeV. The structure is less pronounced in the (n, γ) data [37] compared to the other data sets.

A similar structure was also observed in other nuclei in the $A \approx 200$ mass region. Despite the fact that there is no information on the strength of $M1$ transitions from ARC in ^{196}Pt , the ARC data in this mass region indicate that the $E1$ PSF for $E_\gamma \approx 5$ –7 MeV is stronger than the $M1$ PSF. According to [10] the ratio $f_{E1}/f_{M1} = 4$ –4.5 holds for a majority of $A = 190$ –200 nuclei at energies ≈ 5.5 –6 MeV; the lowest ratio is about 2.9 (for ^{197}Pt). In order to comply with this finding, a realistic PSFs model should have $E1$ PSF significantly higher than the $M1$ PSF at $E_\gamma \gtrsim 5$ MeV.

We decided to test PSFs based on data from all the above-mentioned reactions. As no experimental information is available for $E_\gamma \lesssim 2$ MeV, an extrapolation down to $E_\gamma = 0$ is needed. Usually several different extrapolations were tested; see details below. We further assume that all tested PSFs depend only on E_γ and are—in accord with the Brink hypothesis [40]—independent of any other quantity, such as excitation energy.

1. PSFs based on (n, γ) data

We adopted the $f_{E1} + f_{M1}$ following the experimental points labeled as “ (n, γ) ” and “ARC(BT)” in Fig. 6. We tested a few different extrapolations for $E_\gamma < 2$ MeV and decomposition into $E1$ and $M1$ strength in combination with several NLD models. For decomposition into $E1$ and $M1$ we adopted the $M1$ PSF in the form of either the SF model or a constant (single particle) (with $f_{M1} = 6 \times 10^{-9} \text{ MeV}^{-3}$) and the $E1$ PSF was then calculated as a difference between the experimental points and f_{M1} . Results from two simulations are shown in Fig. 8. Both have the same $M1$ PSF (SF model) and NLD model (Oslo in Fig. 5). The difference is only in the low-energy PSF behavior. The PSFs labeled as “ $n\gamma(\text{const})$ ” uses constant $f_{E1} + f_{M1}$ below $E_\gamma = 2$ MeV, while in the combination “ $n\gamma(0)$ ” the PSF linearly decreases to $f_{E1} + f_{M1} = 0$ for $E_\gamma = 0$.

Although the experimental shapes of MSC spectra are better described, especially for $M = 2$, with these PSFs than with those from Sec. III B, see Fig. 7, the bumps near 2 and 5.6 MeV are still too high in experimental spectra for $M = 3$ and 4. In addition, all the PSF variations based on (n, γ) data overestimate the intensity in the $E_\gamma \approx 2$ –4 MeV in the $M \geq 4$ MSC spectra, which is almost surely a consequence of the excess of the PSF between $E_\gamma = 2$ and 4 MeV visible in the (n, γ) experimental data with respect to the Oslo data; see Fig. 6. These observations indicate that a realistic PSF should exhibit a larger decrease from the bump near 5.6 MeV down to E_γ between about 2 and 4 MeV.

We would like to point out one feature of the simulations that is evident from comparison of the two predictions in Fig. 8. The higher PSF at low E_γ (below 2 MeV in this case) shifts the multiplicity distribution toward higher M . This behavior is intuitive as higher PSFs at low energies increase a

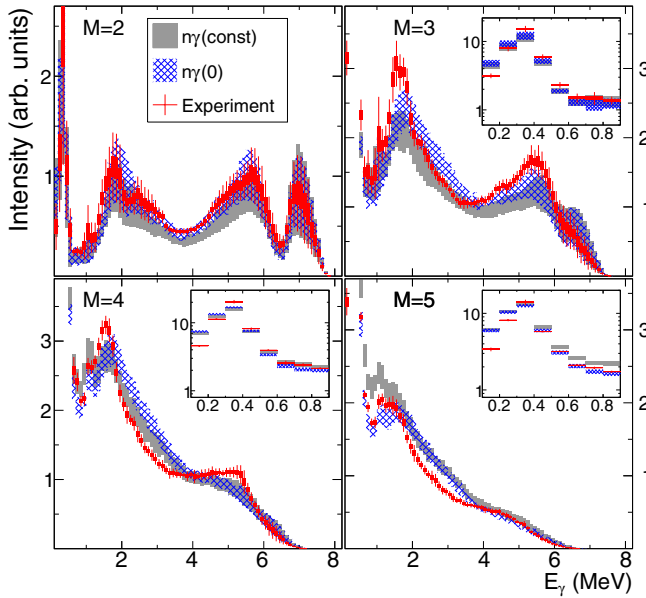


FIG. 8. Comparison of the mean experimental MSC spectra from 1^- resonances with the predictions for the two models described in Sec. III C 1. For the symbol explanation see Fig. 7.

probability for emission of a low- E_γ transitions and will be further examined in Sec. III D 5.

2. PSFs based on NRF data

The PSF from NRF data is available only for $E_\gamma \gtrsim 4.5$ MeV. A PSF extrapolation in a broad E_γ range important for decay is thus necessary. We have tested several different extrapolations; they were based on the *shape* of either the Oslo data or the above-discussed (n, γ) data.

The NRF data overlap with the Oslo data at 4.5 MeV, see Fig. 6(a), which allows the Oslo-based extrapolation from 4.5 MeV down to 2 MeV without any scaling of either data set. A comparison of the mean experimental MSC spectra with predictions using this Oslo-based extrapolation and a constant PSF below 2 MeV, labeled as “NRF,” can be found in Fig. 9. The bump in the PSF near 5.5 MeV is evidently too strong in this model. The same conclusion can be made from simulations with any tested PSF extrapolation below 2 MeV as well as any extrapolation based on the unscaled (n, γ) data.

Further we tested PSFs in which the NRF *shape* was connected at ≈ 5 MeV to *shapes* given by the Oslo or the (n, γ) data. The simulations with PSFs connecting the NRF and the (n, γ) *shapes* result in predictions almost indistinguishable from those discussed in Sec. III C 1 and shown in Fig. 8, no matter what extrapolation was used for $E_\gamma < 2$ MeV. This result is caused by the characteristic dependence of the (n, γ) data between 2 and 4 MeV. Use of the PSFs that connect the NRF *shape* to the Oslo *shape* at ≈ 5 MeV leads to predictions that reproduce the mean experimental MSC spectra very reasonably. Specifically, predictions with the model going through *scaled* NRF data for $E_\gamma \geq 4.8$ MeV, Oslo data for $E_\gamma = 2-4.8$ MeV [black squares in Fig. 6(b)] and a constant PSF for $E_\gamma < 2$ MeV are shown in Figs. 9 and 10. This model

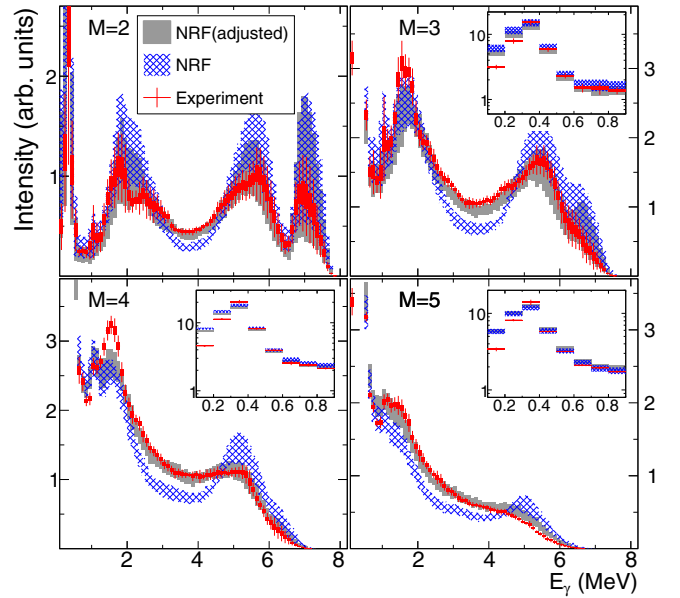


FIG. 9. Comparison of the mean experimental MSC spectra from 1^- resonances with the predictions for the two models described in Sec. III C 2. For the symbol explanation see Fig. 7.

is labeled as “NRF(adjusted),” see the red curves in Fig. 6(b), and is one of the best combinations found in our analysis.

Both simulations shown in Fig. 9 used the Oslo model for NLD and the $M1$ PSF was given by the SF model. Use of different NLD models, different extrapolations for $E_\gamma < 2$ MeV, and different decomposition into $E1$ and $M1$ PSFs leads to similar or worse reproduction of mean experimental MSC spectra.

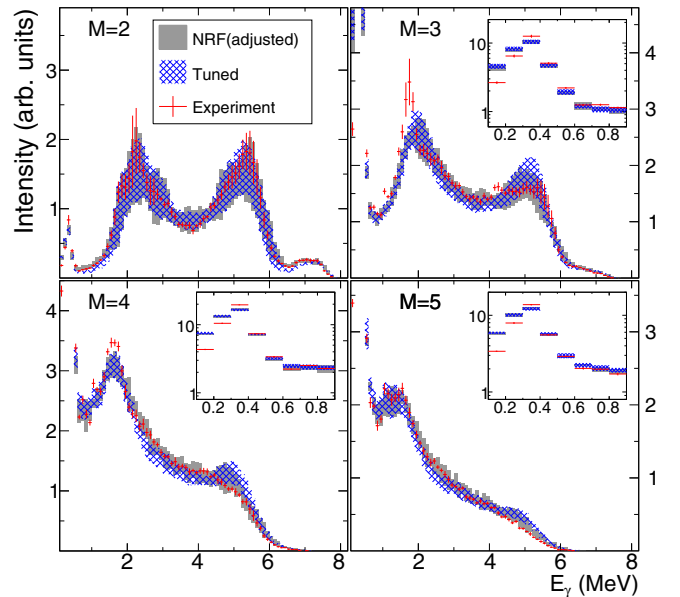


FIG. 10. Comparison of the mean experimental MSC spectra from 0^- resonances with the predictions for the NRF(adjusted) and tuned PSFs. For the symbol explanation see Fig. 7.

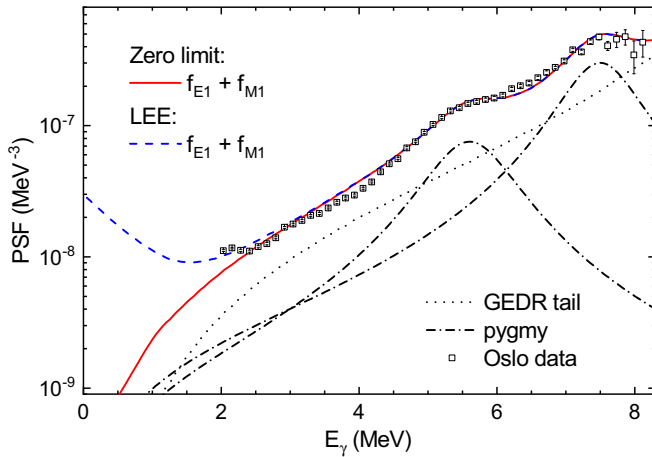


FIG. 11. The Oslo PSF data together with its decomposition based on [8] into the GEDR tail and two pygmy resonances. Two displayed models are introduced in Sec. III D 5.

3. PSFs based on Oslo data

The PSF data from the NRF and Oslo methods differ—depending on the absolute PSF normalization one can either say that the resonance structure near 5.6 MeV is more pronounced in the NRF or that the Oslo data indicate a presence of additional “resonance structure” near 7.5 MeV; see Fig. 6. To preserve the consistency of data from the Oslo experiment, all Oslo-based PSFs should be coupled with the Oslo NLD model as these two quantities are strongly correlated.

The difference in predictions between the NRF(adjusted) and PSFs based on the Oslo data for $E_\gamma \lesssim 6$ MeV is minimal. However, the Oslo-based PSFs significantly overestimate the experimental MSC intensities for $E_\gamma \approx 7$ MeV in $M \leq 3$ spectra if the PSF is dominated by the $E1$ contribution at these high energies (see also Sec. III D 3).

To conclude, the PSFs from no previous study provide a good description of our data. To create PSFs leading to a satisfactory reproduction of our experimental data we have to combine the NRF and Oslo data sets assuming a normalization bias in at least one of the data sets. The resulting NRF(adjusted) PSFs, described in Sec. III C 2, adopt the shape of the Oslo data for $E_\gamma = 2\text{--}4.8$ MeV connected to the shape of the NRF data with appropriate low-energy extrapolation and $E1$ - $M1$ decomposition. In this combination the $E1$ PSF can be regarded as a pygmy resonance on the GEDR tail while the $M1$ PSF is given by a spin-flip resonance.

D. Search for optimum model and additional information on PSFs

Further PSFs tuning was inspired by the interpretation of the Oslo data by the authors of Ref. [8], specifically their decomposition of the PSF data into two pygmy resonances (with maxima at 5.6 and 7.5 MeV and maximum cross sections of 4.9 and 26.1 mb, respectively) and the tail of the GEDR in the form from [41]. The decomposition as well as the sum of individual components, labeled as the “zero limit” model, are visualized in Fig. 11. We tried all combinations of the types

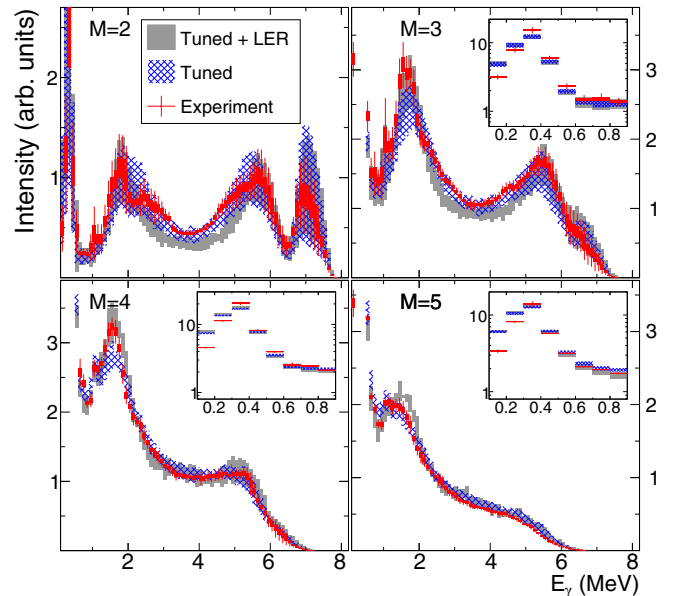


FIG. 12. Comparison of the mean experimental MSC spectra from 1^- resonances with the predictions for the tuned and tuned + LER models. The low-energy resonance (LER) in the $M1$ PSF was centered at 1.8 MeV with the maximum cross section 0.15 mb and resonance width 0.8 MeV. For the symbol explanation see Fig. 7.

of two pygmy resonances and further varied the low-energy PSF dependence below $E_\gamma \approx 3$ MeV again assuming the exact validity of the Brink hypothesis. The resulting model best describing the mean experimental MSC spectra is labeled “tuned” and is shown in Fig. 6. In this model, the pygmy resonance at 5.6 MeV is of the $E1$ type and the $M1$ PSF is mimicked by the tail of the higher-lying resonance. Due to the absence of negative parity levels for $E \lesssim 2$ MeV the simulations are virtually insensitive to the $M1$ PSF for $E_\gamma \gtrsim 6$ MeV. The f_{M1} (and $f_{E1} + f_{M1}$) is thus not shown in the figure for these E_γ . We would like to stress that the resulting $M1$ PSF does not have to be given by the higher-lying resonance from the Oslo analysis [8]. A practically identical $M1$ PSF is given, for instance, by a Lorentzian resonance centered between 6.7 and 7.0 MeV with width of ≈ 2.5 MeV and strength of ≈ 3.5 mb. Such a resonance is much closer to the RIPL-3 systematics [12] for the SF and does not contradict the ARC results [10].

Based on our experience with the MSC spectra, see [13] and references therein, the reproduction of MSC spectra similar to that with the NRF(adjusted) (as shown in Figs. 9 and 10) or with the tuned PSFs (as shown in Figs. 10 and 12) is very good. We usually did not reach better agreement for previously published nuclei. Of course, within the trial and error approach we cannot guarantee that the MSC spectra will not be well described also with rather different combinations of PSFs and NLD models. Nevertheless, we were not able to find a better reproduction of the MSC spectra with any other tested PSFs combination. An illustration of the quality of the reproduction of the sum-energy spectra for the tuned model can be found in Fig. 13. The comparison of differences in MSC predictions with the NRF(adjusted) and tuned PSFs also

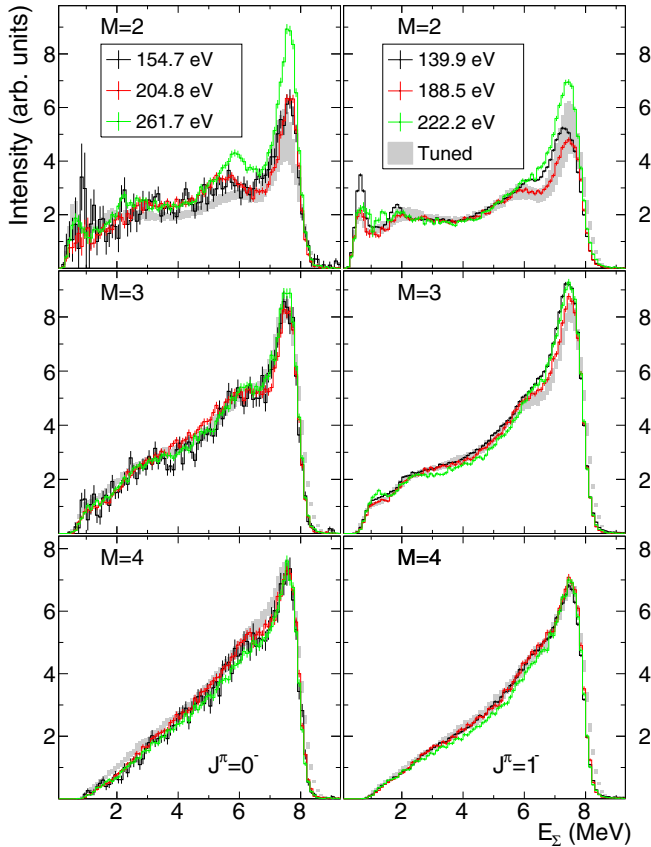


FIG. 13. Comparison of the background-subtracted experimental sum-energy spectra of three 0^- and three 1^- resonances with the predictions for the tuned model. The band from simulations corresponds to $\mu \pm \sigma$ as introduced in Sec. II C. The same resonances as in Fig. 2 are shown.

indicates sensitivity of the spectra to relatively small PSFs changes.

There are only a few regions in the MSC spectra with visible imperfections in the description of experimental spectra with the NRF(adjusted) and tuned PSFs. Specifically, the size of the bump at $E_\gamma \approx 1.6$ MeV is underestimated in the $M \geq 3$ spectra; the effect is very small for $M \geq 5$. We also see slightly higher predicted intensity at higher E_γ in the $M \geq 3$ spectra. Specifically, in the $M \geq 5$ spectra this is the case of both PSFs combinations for $E_\gamma \gtrsim 4$ MeV and in the $M = 3-4$ spectra the NRF(adjusted) PSFs overestimate the intensity at $E_\gamma \gtrsim 6.5$ MeV for $J^\pi = 1^-$ resonances and the tuned model at $E_\gamma \approx 5$ MeV for $J^\pi = 0^-$ resonances. We made various attempts to remove these imperfections in simulations. Some of them are discussed below together with a more detailed analysis of PSFs in different E_γ regions.

1. Attempts to reproduce MSC spectra near 1.6 MeV

The most visible remaining difference between the simulated and experimental MSC spectra is the bump at 1.6 MeV in $M = 3$ and 4. It seems natural that a postulation of a weak low-energy resonance (LER) in the PSF at this energy might lead to a better description of the mean experimental MSC

spectra. Despite many attempts it turns out that a postulation of any resonance structure at these energies, that is able to reproduce the observed bump in the $M = 3$ and 4 spectra, leads to significant changes in other regions. Specifically, as indicated in Fig. 12 with the model combination labeled “tuned + LER,” the predicted intensity is significantly smaller for E_γ between about 2.5 and 5 MeV in the $M = 2$ and 3 spectra and usually the bump near 1.6 MeV is overestimated in the $M \geq 5$ spectra. We conclude that we have not found a better reproduction of the MSC spectra, compared to the NRF(adjusted) or tuned PSFs, with a LER postulated near this energy neither in the $E1$ nor $M1$ PSF.

2. Influence of nuclear level density models

The Oslo NLD model used in the majority of simulations, e.g., those compared above in Figs. 8–12, was based on the Oslo NLD data [30] with applied spin and parity dependence as described in Sec. III A. We also performed simulations using other NLDs shown in Fig. 5. In addition, for the tested NLD models we checked the influence of the parity dependence and the staggering between odd and even spins introduced in Sec. III A.

Use of the parity-independent NLD model above E_c leads to less pronounced bumps near 5.6 MeV (for $M < 5$), to a small shift in the multiplicity distribution to higher values, and especially to problems with predicted spectral intensity at $E_\gamma \approx 4$ MeV in the $M = 2$ spectrum; see also Sec. III D 6. All these changes are due to the significantly different ratio of the number of positive to negative parity levels in the parity-independent model at energies below about 4 MeV.

The reduction of the predicted size of bumps near $E_\gamma = 5.6$ MeV is evidently due to the smaller number of final levels for primary $E1$ transitions at excitation energies 2–3 MeV in the parity-independent NLD model—the number of positive plus negative parity levels is fixed independently of the assumed parity dependence; see Eq. (1). We conclude that the dominance of positive-parity levels at $E \lesssim 4$ MeV is essential for good reproduction of experiment. The acceptable values of parameters for the parity dependence in Eq. (1) are $C_\pi \approx 0.5-2.0$ MeV $^{-1}$ and $\Delta_\pi \approx 3-3.5$ MeV.

With the parity-dependent NLD models the simulations with the BSFG model and the combinatorial NLD shift multiplicity distribution to higher values while simulations with the CT model to slightly lower ones compared to the Oslo NLD model; compare Fig. 14 with Fig. 12. This is a consequence of the fact that the BSFG model (and even more the combinatorial NLD) gives a significantly higher number of levels at intermediate excitation energies ($E \approx 3-7$ MeV) compared to the Oslo and even more to the CT model; see Fig. 5. This increase in the number of levels at intermediate energies allows bypassing the lower-multiplicity cascades through levels just above E_c by higher-multiplicity cascades. With the CT model the predicted MSC spectral shapes are not very different compared to the Oslo NLD model for fixed PSFs models; compare Figs. 14 and 12.

The simulations with the BSFG model underestimate the MSC intensity near 1.6 and 5.6 MeV in $M = 2$ and 3 MSC spectra. This results from the same effect as the

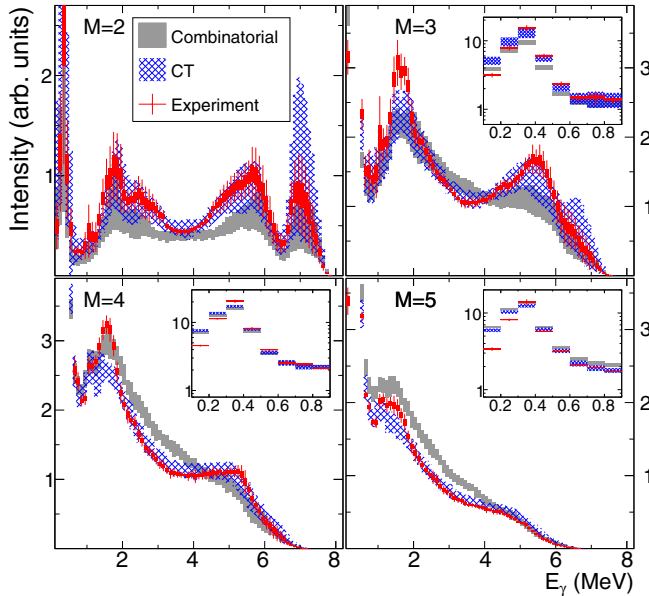


FIG. 14. Comparison of the mean experimental MSC spectra from 1^- resonances with the predictions of the CT NLD model and the combinatorial NLD. The tuned PSF model was used in combination with the CT model, while a model with significantly higher $E1$ PSF near 5.6 MeV, see the text of Sec. III D 2, was combined with the combinatorial NLD. For the symbol explanation see Fig. 7.

multiplicity distribution shift. Additional simulations with the BSFG model indicated that an $E1$ resonance structure shifted from 5.6 MeV towards 6 MeV with the strength at least three times higher than the pygmy resonance of the tuned model is needed to acceptably reproduce the above-mentioned bumps in the MSC spectra. Nevertheless, such a change of the $E1$ PSF induces discrepancies in MSC spectra for higher M .

The combinatorial NLD is so different from the other NLDs used that it predicts very different MSC spectral shapes; see Fig. 14. The combination of this NLD with the tuned PSFs yields predictions similar to those with the QRPA PSFs shown in Fig. 7, i.e., without any clear bumps for $E_\gamma \approx 5.6$ MeV. Absence of the bumps can be (at least partly) understood from Fig. 5. The combinatorial NLD yields the highest number of levels accessible via primary transitions at intermediate excitation energies ($E \approx 3-7$ MeV) out of all tested models. At the same time the number of predicted positive-parity levels is relatively small below about 2.5 MeV. This behavior strongly suppresses the total intensity carried by primary transitions with E_γ close to 5.6 MeV. An enormous PSF enhancement near 5.6 MeV would be required to reproduce the bumps in the MSC spectra, which would introduce other discrepancies in the MSC spectra similarly to the case of the BSFG model. To illustrate the inability of the combinatorial NLD to reproduce bumps in the MSC spectra even with very strong $E1$ PSF near 5.6 MeV, simulations presented in Fig. 14 were performed with the PSFs based on the tuned ones but with the pygmy resonance near 5.6 MeV three times stronger than the original one shown in Fig. 11. Even this strength of the pygmy resonance is far from that which is needed.

For completeness, we should add that we have found no significant influence of the staggering between odd and even spins on predicted MSC spectra.

Due to the complexity of possible changes in NLD (dependence on energy, spin, and parity) and the entanglement with the PSFs models when predicting the MSC spectra, it is rather difficult to make any definite statements related to this quantity. Nevertheless, we can conclude that the excitation energy dependence of the NLD based on the Oslo data [30] combined with significant parity dependence up to relatively high excitation energy seems to be reasonable. With the parity-independent NLD model we have never reached the quality of the description of the experimental MSC spectra as with the parity-dependent one. The combinatorial NLD is not consistent with our data.

3. Photon strength functions at $E_\gamma \gtrsim 6.5$ MeV

As evident from Fig. 6 the E_γ dependencies of PSFs from available experimental data are rather different for $E_\gamma \gtrsim 6$ MeV. Specifically, the Oslo data indicate a significantly steeper dependence than data from other reactions. Exact PSF decomposition into $E1$ and $M1$ is also not known although, as mentioned above, it is expected from ARC data for $E_\gamma \gtrsim 5$ MeV that $E1$ PSF dominates.

The vast majority of the intensity observed in the MSC spectra at these energies is due to the primary transitions. As mentioned above, there are no levels to be fed by $M1$ primary transitions below the excitation energy of about 2 MeV, so the simulations are completely insensitive to f_{M1} at $E_\gamma \gtrsim 6$ MeV. On the other hand, it turns out that the spectral intensity in $M = 2$ (and unreported $M = 1$ from 1^- resonances) MSC spectra is rather sensitive to the relative size of f_{E1} in this region with respect to lower E_γ . As already mentioned in Sec. III C 3, our simulations clearly indicate that the $E1$ shape from the Oslo method [8] is inadequate as it overestimates the MSC intensity for $E_\gamma \gtrsim 6$ MeV. In contrast, the E_γ dependence given by NRF and (n, γ) data, see Fig. 6, is very reasonable. In reality, the f_{E1} at $E_\gamma \gtrsim 6.5$ MeV could be slightly higher than that in the NRF(adjusted) PSFs by about 1/3 of the difference between the Oslo and NRF shapes.

4. Size of the resonance structure near 5.6 MeV

With the tuned PSFs we checked in detail the influence of the size of the pygmy resonance near 5.6 MeV. We found that its maximum cross section surely lies between 2.5 and 6.5 mb, which corresponds to 0.18–0.47% of the Thomas-Reiche-Kuhn sum rule. The required size of the pygmy resonance is partly related to the exact parity dependence of the NLD model; the above-given range was determined using all reasonable possibilities of the parity dependence.

5. Possible low- E_γ enhancement

An interesting feature of PSFs is a possible presence of a low- E_γ enhancement (LEE) previously reported from Oslo-type experiments. Although it has never been observed in nuclei as heavy as Pt, it was recently reported even in Sm nuclei [42].

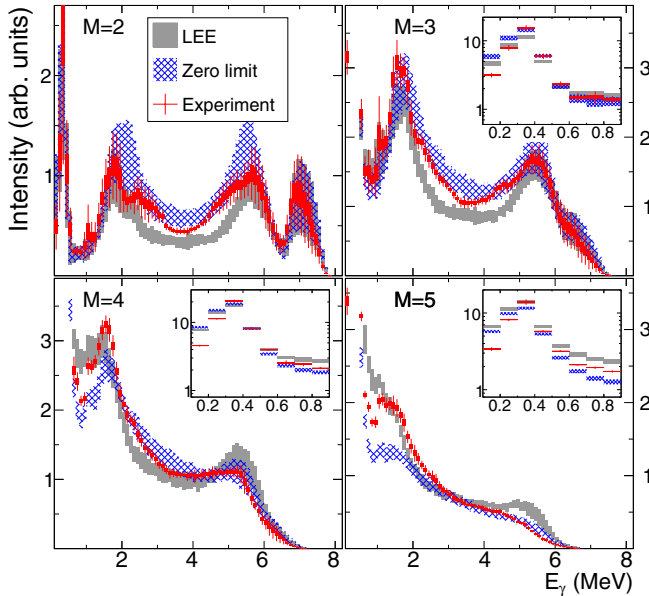


FIG. 15. Comparison of the mean experimental MSC spectra from 1^- resonances with the predictions for the zero limit and LEE models as shown in Fig. 11. For the symbol explanation see Fig. 7.

We tested an influence of the low- E_γ PSFs shape in various forms including constant, linear, and exponential [in the form $f_{\text{LEE}} = f_0 \exp(-E_\gamma/E_s)$] enhancement with different zero- E_γ PSFs limits. The simulated MSC spectra for two PSFs shapes, shown in Fig. 11, are presented in Fig. 15. The zero limit model is the interpretation of the Oslo data by authors of Ref. [8] in terms of two pygmy resonances and the tail of the GEDR. The first pygmy resonance was assumed to be of $E1$ while the second one of the $M1$ type. This model with additional low- E_γ enhancement f_{LEE} is denoted as “LEE”; for the presented simulation the $M1$ transition type with $f_0 = 3 \times 10^{-8} \text{ MeV}^{-3}$ and $E_s = 0.8 \text{ MeV}$ was adopted. We tested also the $E1$ and mixed character of f_{LEE} with different parameters.

The comparison of spectra in Fig. 15 shows clear shifts in the multiplicity distribution—the higher enhancement, the more cascades with higher M —and distorted spectral shapes. The influence of the LEE on the spectra is smaller if the LEE is assumed in the $E1$ PSF (instead of the $M1$ PSF). The reason for smaller sensitivity to $E1$ type comes from the dominance of positive-parity levels at low excitation energies, see Sec. III D 2, and is also thoroughly discussed in Sec. III D 6. We can conclude that the reproduction of experimental MSC spectra requires a presence of nonzero sum $f_{E1} + f_{M1}$ at $E_\gamma \approx 0.5\text{--}3 \text{ MeV}$, which should not significantly differ from a constant. For the (less sensitive) $E1$ type of LEE the f_0 is definitely within $0.5\text{--}2 \times 10^{-8} \text{ MeV}^{-3}$ for $E_s = 0.8 \text{ MeV}$ and $0.2\text{--}4 \times 10^{-8} \text{ MeV}^{-3}$ for $E_s = 0.3 \text{ MeV}$. The limits on the $M1$ LEE are even more strict. Sizable differences are already present for relatively small changes in f_0 especially if the LEE changes the PSF at $E_\gamma \gtrsim 1 \text{ MeV}$. Use of the LEE which influences only transitions with $E_\gamma < 1 \text{ MeV}$, i.e., $E_s \lesssim 0.3 \text{ MeV}$, makes the changes smaller but still visible—our

sensitivity to very low E_γ (below about 0.5 MeV) is limited as transition intensities are proportional to the product $f_{XL} \times E_\gamma^3$.

We would like to note that in the NRF(adjusted) and tuned PSFs, we used the $E1$ -dominated PSFs at low E_γ .

6. PSF composition at intermediate and low E_γ

Although getting information on the PSF decomposition at intermediate and low E_γ is not that straightforward as for $E_\gamma \gtrsim 6.5 \text{ MeV}$, discussed in Sec. III D 3, we can still say something about dipole PSFs for individual transition types.

The $M = 2$ MSC spectrum is dominantly composed of cascades via two γ rays starting from negative-parity resonances and ending at positive-parity low-lying levels. Due to the low spin difference between the resonances and low-lying levels and expected dominance of dipole transitions, the cascades are of $E1$ - $M1$ or $M1$ - $E1$ makeup with the former being more probable. Use of a model with very low $M1$ contribution at $E_\gamma = 3\text{--}5 \text{ MeV}$ (smaller than $E1$ PSF by at least an order of magnitude) leads to a significant underestimation of the intensity in this E_γ region in $M = 2$ spectra, as the competing cascades of higher multiplicities (with first two $E1$ steps) divert the intensity.

Unfortunately, a relatively broad range of ratios f_{E1}/f_{M1} between about 2 and 10 for $E_\gamma \approx 4 \text{ MeV}$ gives predictions that are consistent with experimental data. This can be understood as follows: due to the parity selection rules and the low number of negative parity levels at low excitation energies the influence of the $E1$ PSF is strongly suppressed for transitions below the excitation energy of about $4\text{--}5 \text{ MeV}$. Hence the simulations exhibit low sensitivity to the f_{E1}/f_{M1} ratio for $E_\gamma \approx 4 \text{ MeV}$ but yield significant constraints on the $M1$ PSF shape for these E_γ .

The $M1$ PSF for $E_\gamma \lesssim 5 \text{ MeV}$ increasing with E_γ , similarly to the tail of the SF resonance as shown in Fig. 6(b), is strongly favored. In reality, we cannot unambiguously say if zero limit $f_{M1} = 0$ for $E_\gamma \rightarrow 0$ is required, the $M1$ PSF might flatten for $E_\gamma \lesssim 2 \text{ MeV}$. However, any different $M1$ PSF shape such as a constant PSF, which prefers lower- E_γ transitions, leads to underestimated intensity in the midpart of $M = 2$ MSC spectra, because intermediate levels at $E = 3\text{--}5 \text{ MeV}$ fed directly by primary transitions are forced to decay via transitions with small E_γ and thus contribute to higher M spectra. We would like to note that the dominance of positive-parity levels below about 4 MeV , crucial for the discussion in this section, is essential to reproduce the intensity for $E_\gamma \approx 5.6 \text{ MeV}$ in the MSC spectra; see Sec. III D 2.

If we combine the information on the $M1$ PSF shape at low E_γ with the findings in Sec. III D 5 on the $f_{E1} + f_{M1}$, we can also conclude that the region $E_\gamma \lesssim 2.5 \text{ MeV}$ must be dominated by the $E1$ PSF which is not far from a constant value (at least down to $E_\gamma \approx 0.5 \text{ MeV}$).

Our attempts to improve the description of present experimental data result in the conclusion that the reasonable PSFs are indeed very close to the tuned or NRF(adjusted) PSFs, shown in Fig. 6(b), when combined with the Oslo NLD. We would like to stress that this conclusion is based on the assumption that the PSFs at least approximately follow the Brink hypothesis.

TABLE I. Average total radiative widths $\bar{\Gamma}_\gamma$ (in meV) for NRF(adjusted) and tuned PSFs in combination with different tested NLDs. The parity dependence and the spin staggering were used in the forms introduced in Sec. III A. The uncertainty corresponds to the standard deviation of individual simulated values and thus characterizes the width of the Γ_γ distribution obtained from the DICEBOX simulations.

NLD	NRF(adjusted)		Tuned	
	$J^\pi = 0^-$	$J^\pi = 1^-$	$J^\pi = 0^-$	$J^\pi = 1^-$
CT	63(8)	80(7)	71(9)	87(8)
Oslo	90(10)	106(10)	102(12)	115(10)
BSFG	117(9)	140(7)	134(10)	157(8)
Combinatorial	91(6)	94(5)	107(7)	104(6)

E. Total radiative width

The total radiative width Γ_γ is the only quantity coming from simulations that depends on the absolute values of the PSFs. Its value can be compared to experiment and possibly used for absolute PSF normalizations.

Instead of PSF normalizations we rather decided to show, with fixed PSFs, a dependence of the predicted average $\bar{\Gamma}_\gamma$ on other quantities. First, there is a significant dependence on the NLD model, which can be seen from the values of $\bar{\Gamma}_\gamma$ with NRF(adjusted) and tuned PSFs listed in Table I. This dependence complicates the possible absolute normalizations of PSFs unless the appropriate NLD is fixed independently. Second, the calculated $\bar{\Gamma}_\gamma$'s also indicate a non-negligible dependence on the resonance spin; the only exception is the combinatorial NLD with very different spin distribution compared to the other NLDs. Such a dependence can be expected as a significant fraction of $\bar{\Gamma}_\gamma$ comes from transitions to low-lying levels (below about 2 MeV of excitation energy). The absence of 1^+ states at these excitation energies leads to smaller $\bar{\Gamma}_\gamma$ from 0^- resonances. Although usually only the spin-independent average value of $\bar{\Gamma}_\gamma$ is listed in the literature, see, e.g., [12,24], de Barros *et al.* [43] tried to determine $\bar{\Gamma}_\gamma$ separately for resonances with both spins and arrived at 93(10) and 118(6) meV for 0^- and 1^- resonances, respectively. The observed relative difference in values for the two spins is, within uncertainties, consistent with the differences shown in Table I.

As the $\bar{\Gamma}_\gamma$'s predicted for the NRF(adjusted) and tuned PSFs in combination with the Oslo NLD are close to the evaluated values of 122(20) and 120(20) meV from Refs. [12,24], respectively, the absolute PSFs values used in this paper seem to be reasonable. However, as evident from Table I, the absolute values of PSFs would change if a different NLD model was found appropriate.

IV. FLUCTUATION PROPERTIES OF MSC SPECTRA

In the statistical model the PT distribution is assumed for the decay of all levels above the critical energy E_c . Within our framework this assumption can be tested by comparing the experimental and simulated fluctuations of MSC spectra. The

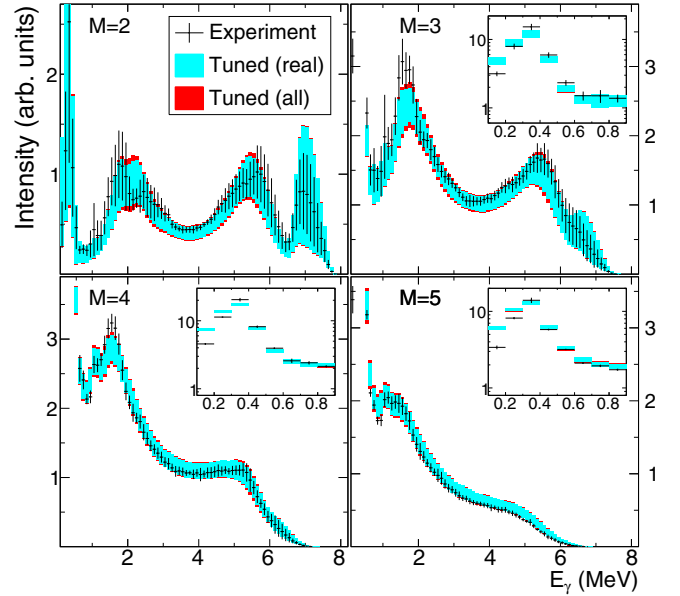


FIG. 16. Comparison of MSC intensities and their fluctuations from experiment and extended simulations for 1^- resonances. Black symbols indicate $I_{\text{exp}} \pm \phi_{\text{exp}}$ obtained from the ML fit as described in Sec. II B. The cyan band corresponds to $\mu \pm \phi$ and the red band to $\mu \pm \sqrt{\phi^2 + \Phi^2}$ as deduced from extended simulations with the tuned PSFs and Oslo NLD model.

number of 1^- resonances, for which we were able to prepare the MSC spectra, allows us to check also the fluctuations of individual MSC intensities. The fluctuation analysis was, for the first time, performed for two even-even Dy isotopes in [22]. Observed differences among experimental MSC spectra from different resonances seemed to be systematically smaller than fluctuations predicted in simulations. This fact might indicate that the use of the PT distribution for description of fluctuations of individual transition intensities is inadequate.

Similarly to Ref. [22] we have performed extended simulations with $I = 40$ nuclear realizations within each of $K = 20$ nuclear suprealizations. These time-consuming calculations were made only for the tuned PSFs in combination with the Oslo and CT NLD models, which seem to provide a satisfactory description of the mean experimental MSC spectra. Specifically, for each suprealization k we determined quantities μ_k and ϕ_k introduced in Sec. II C again using the ML approach with the ML function analogous to Eq. (A2). The validity of assumption of the normal distribution of individual values μ_{ik} for fixed k was checked beforehand. Although applied statistical tests sometimes showed a deviation from the normal distribution, we can claim that in energy bins between E_c and $S_n - E_c$ in $M = 2$ spectra and in all bins with the MSC intensity significantly higher than zero in multiplicities $M \geq 3$ the distribution of MSC intensities is so close to the normal distribution that this form of the ML function is a well justified approximation. Nevertheless, for the sake of clarity we show the full energy ranges of MSC spectra in Figs. 16 and 17.

The distribution of the set $\{\phi_k\}_{k=1}^K$ from the ML approach is reasonably narrow with almost all values falling into $\phi \pm 30\%$ interval in all these energy bins. As a result it seems

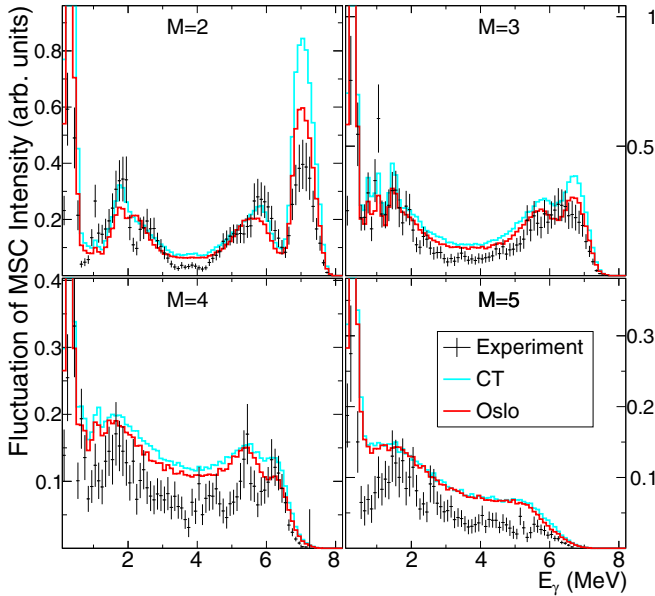


FIG. 17. Comparison of fluctuations of experimental MSC intensities ϕ_{exp} (black symbols) with the average fluctuation within suprealizations ϕ (cyan and red lines) for the tuned PSFs in combination with CT and Oslo NLD models, respectively.

appropriate to use the value of ϕ instead of the distribution of ϕ_k when comparing with experimental fluctuations. We have made additional tests as in Ref. [22], most importantly there are no significant correlations between fluctuations due to nuclear realizations and due to nuclear suprealizations, i.e., the quantities Φ and ϕ are statistically independent and can be extracted separately from our extended simulations for the above-mentioned E_γ bins.

It turns out that the fluctuation of means Φ is about an order of magnitude lower than the fluctuation of intensities from individual resonances ϕ for all checked energy bins, as shown by the difference between the red and cyan fill in Fig. 16. Small values of Φ (as compared to ϕ) can be used as a justification of the approach used in Sec. III for testing the adequacy of different PSFs models. The distribution of intensities from individual nuclear suprealizations used there is representative of the distribution from different realizations within a fixed suprealization.

Assuming that the fluctuations are correctly described in our simulations, we should not only require agreement between the mean experimental and simulated MSC intensity, but also the estimate of fluctuations ϕ from simulations, represented by cyan bands in Fig. 16, should be comparable to the estimate of fluctuations of experimental MSC intensities ϕ_{exp} , given as error bars in Fig. 4.

The fluctuations from two extended simulations and experiment are compared in Fig. 17. The expectation values of simulated fluctuations are on average higher than their experimental counterparts for $M \geq 3$ spectra. The ratio of the two fluctuations seems to be often in the range of ≈ 1.5 – 2 . In the $M = 2$ spectrum there is a significant oscillation of the ratios for different energy regions.

Although the difference in fluctuations might indicate their inadequate treatment in simulations we have a couple of comments on the presented results. First, there is often a significant correlation in values in several neighboring bins as the energy resolution of the detector is usually worse than 100 keV. Second, the tested model combination does not reproduce experimental spectra perfectly; see Fig. 16. It is expected that simulated fluctuations do depend on the adopted combination of PSFs and especially NLD models—a different number of simulated levels in the excitation energy interval corresponding to the E_γ range can significantly change the simulated fluctuations ϕ therein. This effect is visible in Fig. 17—simulations with the CT NLD model, which yields a smaller number of levels than the Oslo NLD model in the whole range of energies, show systematically higher ϕ at least in $M = 3$ – 4 . Furthermore, while the assumptions used in the DICEBOX code seem to be well justified for highly excited states such as neutron resonances, there might be additional nonstatistical effects in the decay of levels at energies just above E_c , which might also be responsible for our inability to perfectly reproduce the MSC spectra.

As a result, it seems rather difficult to make any definite conclusions about the validity of the PT fluctuations of individual transition intensities in ^{196}Pt . Nevertheless, this measurement shows the same tendency observed in Dy [22]. Namely, the simulations produce slightly higher fluctuations than are supported by the data.

V. SUMMARY

The coincident measurement of γ rays from s -wave neutron resonances in the $^{195}\text{Pt}(n, \gamma)$ reaction was performed using the enriched Pt target at the DANCE detector array of the LANSCE spallation neutron source. The multistep γ cascade spectra for different multiplicities from five $J^\pi = 0^-$ and 11 $J^\pi = 1^-$ neutron resonances were used to test the validity of various PSFs and NLD models. The number of $J^\pi = 1^-$ resonances also allowed us to check the size of observed and predicted fluctuations of MSC intensities.

The behavior of the experimental spectra, in particular of the strong primary transitions with $E_\gamma \approx 5.6$ MeV from different resonances, can be described within the concept of the statistical model and photon strength functions. The PSFs describing well the ^{196}Pt data must have a resonancelike structure in the $E1$ PSF at γ -ray energies near 5.6 MeV that has been reported in $A \approx 200$ nuclei from other experimental techniques in the past.

The CT and Oslo NLDs are favored over the BSFG model and combinatorial calculation. The best description of experimental spectra was found when using the parity dependent NLDs at least below an excitation energy of 4 MeV. On the other hand, our data are insensitive to the staggering between odd and even spins.

Although there could be some dependence on the choice from acceptable NLD models, the size of the resonance structure at 5.6 MeV seems to be comparable to that reported earlier from Oslo-type experiment [8] and about a half of the strength reported from NRF data [7]. The Oslo data at energies $E_\gamma \gtrsim 6.5$ MeV are excluded if interpreted as an $E1$ resonance

and it is in contradiction with findings from average resonance capture experiments if interpreted as an $M1$ resonance. On the other hand, the *shape* of NRF data at these E_γ provides a very good description of experimental spectra. Overall, the PSF from (n, γ) measurements as compiled in Ref. [4] seems inappropriate. Our analysis further shows that there is no sizable low- E_γ PSF enhancement; the most appropriate shapes for $E_\gamma \lesssim 2$ MeV are a constant $E1$ PSF and a spin-flip Lorentzian-tail-like $M1$ PSF.

The size of fluctuations among experimental MSC intensities from different neutron resonances with $J^\pi = 1^-$ is slightly smaller than the simulated one for the vast majority of γ -ray energies. This finding is consistent with the results on two even-even Dy isotopes—the first case where the fluctuations were analyzed. Although this observation may point towards the invalidity of the Porter-Thomas distribution for fluctuations of individual primary transition intensities, the situation is more complicated due to the imposed assumptions. In any case further investigation of this phenomenon is necessary.

ACKNOWLEDGMENTS

This work benefited from the use of the LANSCE accelerator facility and was supported by the US Department of Energy through the Los Alamos National Laboratory. Los Alamos National Laboratory is operated by Triad National Security, LLC, for the National Nuclear Security Administration of US Department of Energy (Contract No. 89233218CNA000001). It was also supported by Czech Science Foundation Project No. 19-14048, the Charles University Projects No. UNCE/SCI/013 and No. GAUK 590218, and by International Atomic Energy Agency Project No. IAEA CRP F41032. N.S. acknowledges the support of JINR-Czech Student Program. The ^{195}Pt isotope used in this research was supplied by the United States Department of Energy Office of Science by the Isotope Program in the Office of Nuclear Physics.

APPENDIX: EXPERIMENTAL OBSERVABLES AND THEIR SIMULATED COUNTERPARTS

The way of calculating the measures of observables from experimental data and their simulated counterparts are given in this Appendix.

1. Details on the mean experimental MSC spectra

For $J^\pi = 1^-$ resonances we adopted the procedure introduced in Ref. [22]. Specifically, we computed, for each E_γ bin, the *mean experimental MSC intensity* I_{exp} and the *fluctuation of experimental MSC intensities* ϕ_{exp} using a maximum likelihood (ML) fit of the set of (normalized and background-subtracted) experimental MSC intensities from $L_{\text{exp}} = 11$ individual resonances λ . The experimental intensity in each bin is for each resonance characterized by its mean I_λ and uncertainty Δ_λ .

For the ML fit we assumed that the probability density function describing the distribution of experimental MSC intensities I_λ is a normal distribution. Hence the likelihood

function \mathcal{L} was defined as

$$\mathcal{L} = \prod_{\lambda=1}^{L_{\text{exp}}} \frac{1}{\sqrt{2\pi(\Delta_\lambda^2 + \phi_{\text{exp}}^2)}} \exp\left[-\frac{(I_\lambda - I_{\text{exp}})^2}{2(\Delta_\lambda^2 + \phi_{\text{exp}}^2)}\right] h(\Delta_\lambda), \quad (\text{A1})$$

where $h(\Delta_\lambda)$ is the error distribution.

2. Details on the simulated MSC spectra

Simulations of individual γ cascades deexciting neutron resonances with specific J^π were performed utilizing the Monte Carlo DICEBOX algorithm [27,28]. Let us call any simulated set of levels and intensities of all transitions as a *nuclear realization* and a specific set of realizations with identical levels below S_n and identical intensities of secondary transitions as a *nuclear suprealization*. The detailed description of the DICEBOX algorithm, that includes nuclear realizations and suprealizations, can be found in Ref. [28] and specific details of application of the algorithm to simulations of MSC spectra in [22]. This concept allows (in favorable conditions) separation of two different sources of fluctuations present in simulations. The first type of fluctuations is caused by the PT fluctuations of primary transitions—in the actual nucleus the decays of different neutron resonances of the same spin and parity differ only in intensities of primary transitions while all levels and intensities of secondary transitions are identical. However, the exact positions of levels below S_n as well as intensities of secondary transitions are not known. To overcome this we randomly simulate a number of artificial nuclei, which differ in individual levels coming from random discretization of the NLD formula and their decay. This difference introduces the second type of fluctuations.

From simulations of $i = 1, \dots, I$ nuclear realizations within each of $k = 1, \dots, K$ nuclear suprealizations we can get the following measures for any observable μ_{ik} : (i) μ as the mean value, (ii) μ_k as the mean over realizations within a given suprealization k , (iii) Φ as the size of fluctuations of means μ_k over suprealizations, (iv) ϕ_k as the size of fluctuations of μ_{ik} over realizations i in a given suprealization k , and (v) ϕ^2 as the average of ϕ_k^2 over suprealizations k . There are different ways to calculate these measures, e.g., simple averaging or maximum likelihood fits. For the purpose of this paper we used the latter option. We assume that the observable μ_{ik} corresponds to the simulated normalized intensity in a bin of a MSC spectrum. The simulated MSC spectra were constructed in the same way as their experimental counterparts.

During the search for appropriate models of PSFs and NLD in Sec. III we simulated $I = 1$ nuclear realization within each of $K = 20$ nuclear suprealizations for each model combination. For this choice of K and I not all above-mentioned measures can be deduced. We determined the value μ and the overall fluctuation σ of individual $\mu_k \equiv \mu_{1k}$ using the ML method assuming again their normal distribution:

$$\mathcal{L}_{\text{sim}} = \prod_{k=1}^K \frac{1}{\sqrt{2\pi(\mu_k/L + \sigma^2)}} \exp\left[-\frac{(\mu_k - \mu)^2}{2(\mu_k/L + \sigma^2)}\right], \quad (\text{A2})$$

where the term μ_k/L reflects the Poisson uncertainty of Monte Carlo counting. Unless specified otherwise $L = 2 \times 10^5$ random γ cascades were generated within each nuclear realization.

The case of more time-consuming extended simulations, that were made only for a few model combinations and 1^- resonances, with $K = 20$ and $I = 40$ is discussed in Sec. IV. The full information on the quantities (i)–(v) defined above was obtained and comparison to the fluctuations

of experimental MSC intensities ϕ_{exp} allows us to draw some conclusions not only about the validity of different models of PSFs and NLD but also about adequacy of PT fluctuations.

The assumption on normal distribution of values μ_{ik} used in the ML fit seems to be reasonable for a majority of bins in MSC spectra but it is definitely incorrect at the wings of $M = 2$ spectra, where the dominant contribution comes from cascades via a few well-separated levels.

-
- [1] G. J. Mathews and R. A. Ward, *Rep. Prog. Phys.* **48**, 1371 (1985).
- [2] C. Sneden, J. J. Cowan, and R. Gallino, *Annu. Rev. Astron. Astrophys.* **46**, 241 (2008).
- [3] Report of the Nuclear Physics and Related Computational Science R&D for Advanced Fuel Cycles Workshop, August 10-12, 2006, Bethesda, Maryland (2006), <https://www.osti.gov/biblio/1298979>.
- [4] G. A. Bartholomew, E. D. Earle, A. J. Ferguson, J. W. Knowles, and M. A. Lone, *Adv. Nucl. Phys.* **7**, 229 (1973).
- [5] S. Joly, D. M. Drake, and L. Nilsson, *Phys. Rev. C* **20**, 2072 (1979).
- [6] M. Igashira, H. Kitazawa, M. Shimizu, H. Komano, and N. Yamamuro, *Nucl. Phys. A* **457**, 301 (1986).
- [7] R. Massarczyk, G. Schramm, A. R. Junghans, R. Schwengner, M. Anders, T. Belgya, R. Beyer, E. Birgersson, A. Ferrari, E. Grosse, R. Hannaske, Z. Kis, T. Kogler, K. Kosev, M. Marta, L. Szentmiklosi, A. Wagner, and J. L. Weil, *Phys. Rev. C* **87**, 044306 (2013).
- [8] F. Giacoppo, F. L. Bello Garrote, T. K. Eriksen, A. Gørgen, M. Guttormsen, T. W. Hagen, A. C. Larsen, B. V. Kheswa, M. Klintefjord, P. E. Koehler, L. G. Moretto, H. T. Nyhus, T. Renstrøm, E. Sahin, S. Siem, and T. G. Tornyi, *EPJ Web Conf.* **93**, 01039 (2015).
- [9] F. Giacoppo, F. L. Bello Garrote, L. A. Bernstein, D. L. Bleuel, R. B. Firestone, A. Gørgen, M. Guttormsen, T. W. Hagen, M. Klintefjord, P. E. Koehler, A. C. Larsen, H. T. Nyhus, T. Renstrøm, E. Sahin, S. Siem, and T. Tornyi, *Phys. Rev. C* **91**, 054327 (2015).
- [10] J. Kopecky, S. Goriely, S. Péru, S. Hilaire, and M. Martini, *Phys. Rev. C* **95**, 054317 (2017).
- [11] D. Savran, T. Aumann, and A. Zilges, *Prog. Part. Nucl. Phys.* **70**, 210 (2013).
- [12] R. Capote, M. Herman, P. Obložinsky, P. Young, S. Goriely, T. Belgya, A. Ignatyuk, A. Koning, S. Hilaire, V. Plujko, M. Avrigeanu, O. Bersillon, M. Chadwick, T. Fukahori, Z. Ge, Y. Han, S. Kailas, J. Kopecky, V. Maslov, G. Reffo *et al.*, *Nucl. Data Sheets* **110**, 3107 (2009).
- [13] M. Krčička, S. Goriely, S. Hilaire, S. Peru, and S. Valenta, *Phys. Rev. C* **99**, 044308 (2019).
- [14] S. Goriely, *Phys. Lett. B* **436**, 10 (1998).
- [15] M. Heil, R. Reifarth, M. M. Fowler, R. C. Haight, F. Kappeler, R. S. Rundberg, E. H. Seabury, J. L. Ullmann, J. B. Wilhelmy, and K. Wisshak, *Nucl. Instrum. Methods Phys. Res., Sect. A* **459**, 229 (2001).
- [16] R. Reifarth, T. A. Bredeweg, A. Alpizar-Vicente, J. C. Browne, E. I. Esch, U. Greife, R. C. Haight, R. Hatarik, A. Kronenberg, J. M. O'Donnell, R. S. Rundberg, J. L. Ullmann, D. J. Vieira, J. B. Wilhelmy, and J. M. Wouters, *Nucl. Instrum. Methods Phys. Res., Sect. A* **531**, 530 (2004).
- [17] P. W. Lisowski and K. F. Schoenberg, *Nucl. Instrum. Methods Phys. Res., Sect. A* **562**, 910 (2006).
- [18] M. Mocko and G. Muhrer, *Nucl. Instrum. Methods Phys. Res., Sect. A* **704**, 27 (2013).
- [19] M. Jandel, T. A. Bredeweg, A. Couture, M. M. Fowler, E. M. Bond, M. B. Chadwick, R. R. C. Clement, E. I. Esch, J. M. O'Donnell, R. Reifarth, R. S. Rundberg, J. L. Ullmann, D. J. Vieira, J. B. Wilhelmy, J. M. Wouters, R. A. Macri, C. Y. Wu, and J. A. Becker, *Nucl. Instrum. Methods Phys. Res., Sect. B* **261**, 1117 (2007).
- [20] J. M. Wouters, A. A. Vicente, T. A. Bredeweg, E. Esch, R. C. Haight, R. Hatarik, J. M. O'Donnell, R. Reifarth, R. S. Rundberg, J. M. Schwantes, S. A. Sheets, J. L. Ullmann, D. J. Vieira, and J. B. Wilhelmy, *IEEE Trans. Nucl. Sci.* **53**, 880 (2006).
- [21] M. Jandel, T. A. Bredeweg, E. M. Bond, M. B. Chadwick, R. R. Clement, A. Couture, J. M. O'Donnell, R. C. Haight, T. Kawano, R. Reifarth, R. S. Rundberg, J. L. Ullmann, D. J. Vieira, J. B. Wilhelmy, J. M. Wouters, U. Agvaanluvsan, W. E. Parker, C. Y. Wu, and J. A. Becker, *Phys. Rev. C* **78**, 034609 (2008).
- [22] S. Valenta, B. Baramsai, T. A. Bredeweg, A. Couture, A. Chyżh, M. Jandel, J. Kroll, M. Krčička, G. E. Mitchell, J. M. O'Donnell, G. Rusev, J. L. Ullmann, and C. L. Walker, *Phys. Rev. C* **96**, 054315 (2017).
- [23] S. A. Sheets, U. Agvaanluvsan, J. A. Becker, F. Bečvář, T. A. Bredeweg, R. C. Haight, M. Jandel, M. Krčička, G. E. Mitchell, J. M. O'Donnell, W. Parker, R. Reifarth, R. S. Rundberg, E. I. Sharapov, J. L. Ullmann, D. J. Vieira, J. B. Wilhelmy, J. M. Wouters, and C. Y. Wu, *Phys. Rev. C* **79**, 024301 (2009).
- [24] S. F. Mughabghab, *Atlas of Neutron Resonances* (Elsevier, Amsterdam, 2006).
- [25] F. Bečvář, P. E. Koehler, M. Krčička, G. E. Mitchell, and J. L. Ullmann, *Nucl. Instrum. Methods Phys. Res., Sect. A* **647**, 73 (2011).
- [26] C. E. Porter and R. G. Thomas, *Phys. Rev.* **104**, 483 (1956).
- [27] F. Bečvář, *Nucl. Instrum. Methods Phys. Res., Sect. A* **417**, 434 (1998).
- [28] M. Krčička, S. Valenta, and F. Bečvář (unpublished).
- [29] H. Xiaolong, *Nucl. Data Sheets* **108**, 1093 (2007).
- [30] F. Giacoppo, F. L. Bello Garrote, L. A. Bernstein, D. L. Bleuel, T. K. Eriksen, R. B. Firestone, A. Gørgen, M. Guttormsen,

- T. W. Hagen, B. V. Kheswa, M. Klintefjord, P. E. Koehler, A. C. Larsen, H. T. Nyhus, T. Renstrøm, E. Sahin, S. Siem, and T. Tornyi, *Phys. Rev. C* **90**, 054330 (2014).
- [31] A. C. Larsen, M. Guttormsen, M. Krtička, E. Běták, A. Bürger, A. Görge, H. T. Nyhus, J. Rekstad, A. Schiller, S. Siem, H. K. Toft, G. M. Tveten, A. V. Voinov, and K. Wikan, *Phys. Rev. C* **83**, 034315 (2011); **97**, 049901(E) (2018).
- [32] T. von Egidy and D. Bucurescu, *Phys. Rev. C* **80**, 054310 (2009).
- [33] S. Goriely, S. Hilaire, and A. J. Koning, *Phys. Rev. C* **78**, 064307 (2008).
- [34] S. I. Al-Quraishi, S. M. Grimes, T. N. Massey, and D. A. Resler, *Phys. Rev. C* **67**, 015803 (2003).
- [35] T. von Egidy and D. Bucurescu, *Phys. Rev. C* **78**, 051301(R) (2008).
- [36] M. Martini, S. Péru, S. Hilaire, S. Goriely, and F. Lechaftois, *Phys. Rev. C* **94**, 014304 (2016).
- [37] L. V. Groshev, A. M. Demidov, V. I. Pelekhov, L. L. Sokolovskii, G. A. Bartholomew, A. Doveika, K. M. Eastwood, and S. Monaro, *Nucl. Data Tables* **A5**, 243 (1969).
- [38] L. M. Bollinger and G. E. Thomas, *Phys. Rev. Lett.* **18**, 1143 (1967).
- [39] J. A. Cizewski, R. F. Casten, G. J. Smith, M. R. Macphail, M. L. Stelts, W. R. Kane, H. G. Börner, and W. F. Davidson, *Nucl. Phys. A* **323**, 349 (1979).
- [40] D. Brink, Ph.D. thesis, University of Oxford, 1955.
- [41] S. Goriely and E. Khan, *Nucl. Phys. A* **706**, 217 (2002).
- [42] A. Simon, M. Guttormsen, A. C. Larsen, C. W. Beausang, P. Humby, J. T. Burke, R. J. Casperson, R. O. Hughes, T. J. Ross, J. M. Allmond, R. Chyzh, M. Dag, J. Koglin, E. McCleskey, M. McCleskey, S. Ota, and A. Saastamoinen, *Phys. Rev. C* **93**, 034303 (2016).
- [43] S. de Barros, V. D. Huynh, J. Julien, J. Morgenstern, and C. Samour, *Nucl. Phys. A* **131**, 305 (1969).